

# Tailored Synthesis of the Narrowest Zigzag Graphene Nanoribbon Structure by Compressing the Lithium Acetylide under High Temperature

Xiao Dong,<sup>†</sup> Lijuan Wang,<sup>†</sup> Kuo Li,<sup>\*,†,‡</sup> Haiyan Zheng,<sup>\*,†,‡</sup> Yajie Wang,<sup>†</sup> Yue Meng,<sup>‡</sup> Haiyun Shu,<sup>†</sup> Ho-kwang Mao,<sup>†,§</sup> Shaomin Feng,<sup>||,⊥</sup> and Changqing Jin<sup>||,⊥</sup>

<sup>†</sup>Center for High Pressure Science and Technology Advanced Research, 100094 Beijing, China

<sup>‡</sup>HPCAT, X-Ray Science Division, Argonne National Lab, Argonne, Illinois 60439, United States

<sup>§</sup>Geophysical Lab, Carnegie Institution of Washington, Washington, D.C. 20015, United States

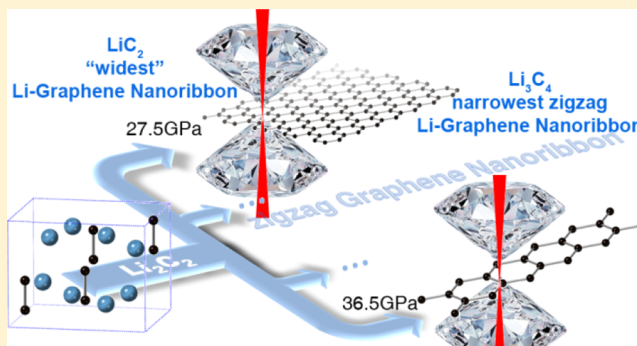
<sup>||</sup>Institute of Physics, Chinese Academy of Sciences, Beijing 100190, China

<sup>⊥</sup>Collaborative Innovation Centre of Quantum Matter, Beijing 100190, China

HPSTAR  
614-2018

## Supporting Information

**ABSTRACT:** Scientists are searching for the goal-directed methods to synthesize graphene nanoribbons (GNRs) with a particular edge type and width, which determines their electronic transport properties. A series of Li zigzag GNRs (ZGNRs) with different widths were predicted under high pressure with a stoichiometric ratio of  $\text{Li}_{n+1}\text{C}_{2n}$ , which indicates a route to prepare ultranarrow GNRs. Here, with thermodynamics and ab initio Gibbs free-energy calculations by quasi-harmonic approximation, we investigated the phase stabilities of the Li GNR compounds under high pressure and high temperature. We have also identified Li graphenide  $\text{LiC}_2$  ( $n = \infty$ ) and Li polyacetylide  $\text{Li}_3\text{C}_4$  ( $n = 2$ ) experimentally at the predicted pressure and temperature conditions using in situ X-ray diffraction, which can be recognized as the two end members of  $\text{Li}_{n+1}\text{C}_{2n}$  with the widest and narrowest ZGNR structures. High temperature and the temperature gradient increased the degree of polymerization and facilitated the formation of wider GNR or carbon slices. This suggests that by controlling temperature and pressure, we may get ultranarrow Li ZGNRs composed of a limited number of parallel carbon chains, such as 3- or 4-zigzag GNR, which is ready to be protonated or functionalized to form atomically ordered ZGNRs.



## INTRODUCTION

Graphene nanoribbons (GNRs), defined as strips of graphene, exhibit exceptional electronic, optical, and magnetic properties.<sup>1–3</sup> The quantum confinement nature of GNRs offers tunable band gaps, which can be modified by the width and edge structure (zigzag, armchair, or mixed).<sup>4,5</sup> Among the GNRs, the ultranarrow GNRs, constructed by several parallel carbon chains, have band gaps comparable to typical semiconductors and have potential applications in high-performance field-effect transistors.<sup>6–9</sup> Currently, the ultranarrow GNRs can only be controllably synthesized by “bottom-up” chemical methods, instead of “top-down” methods such as cutting and unzipping the graphite or carbon nanotubes.<sup>10–12</sup> The “bottom-up” approach can control and modify the width and edge structure at the atomic scale, and the typical reaction is an aryl–aryl coupling, followed by cyclodehydrogenation.<sup>13</sup> However, such reactions are severely limited by the solubility of oligophenylene, as well as the reactivity and regioselectivity.<sup>14–17</sup> Only appropriate precursors

can scalably react to produce GNRs and their products are typically armchair GNRs or coved zigzag GNRs (ZGNRs), as reviewed in the literature.<sup>18,19</sup> For ideal ZGNRs, there are very few examples, including the 6-ZGNR constructed by six zigzag chains<sup>20</sup> and 2-ZGNR (polyacenes).<sup>21–23</sup> As the narrowest ZGNR, polyacene is even more difficult to be synthesized, and the longest pure polyacene is heptacene ([7]ac).<sup>21</sup> Even if including those stabilized by the matrix or surface, the longest polyacene has only 11 hexagonal rings (undecacene, [11]ac).<sup>24</sup> Because the electronic properties of ultranarrow ZGNRs are significantly affected by the edge states, precise synthesis with clean, easily modified, and designed edges is of great interest, and the synthesis techniques still need to be developed.

Carbide is recognized as an important precursor to synthesize novel carbon allotropes, such as graphene, nano-

Received: April 30, 2018

Revised: August 7, 2018

Published: August 13, 2018

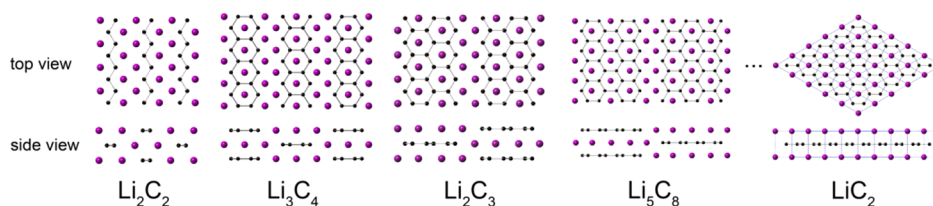


**Figure 1.** Predicted crystal structures of  $\text{Li}_{n+1}\text{C}_{2n}$  ( $n = 1, 2, \dots$ ). The black and purple spheres represent the carbon and lithium atoms, respectively.

tubes, and nanodiamonds.<sup>25</sup> Inspired by several successful synthesized silicon and germanium allotropes from the metal silicide or germanide,<sup>26</sup> pure novel carbon allotropes can be expected after leaching the metal atoms from specific metal carbides. Theoretically, carbon atoms in metal carbides can form a chain, ribbon, graphene sheet, and three-dimensional structure under high pressure.<sup>27–30</sup> Among these, several lithium ZGNRs were predicted, such as  $\text{Li}_2\text{C}_2$  (ribbon, *Cmcm*),  $\text{Li}_3\text{C}_4$ , and  $\text{Li}_2\text{C}_3$  ( $\text{Li}_4\text{C}_6$ ).<sup>29</sup> These compounds have a common structural feature, that is, carbon ribbon constructed by antiphase parallel zigzag chains. On this basis, a broad range of compounds which have a general formula  $\text{Li}_{n+1}\text{C}_{2n}$  ( $n = 1, 2, \dots$ ) can be proposed (Figure 1). For example,  $\text{Li}_2\text{C}_2$  (chain),  $\text{Li}_3\text{C}_4$ , and  $\text{Li}_2\text{C}_3$  contain 1, 2, and 3 chains, respectively (Figure 1). These ZGNRs are stacked perpendicularly to their planes, with Li sandwiched between two six-membered rings of neighboring ribbons and between the two half-rings on the edges (Figure 1).

Thus, following this rule, we can expect zigzag ribbon structures with any width, from a chain ( $n = 1$ ) to sheet ( $n = \infty$ ), which in principle have infinite length and identical edges. In our previous study, some polycarbide anions were identified when compressing  $\text{Li}_2\text{C}_2$  into an amorphous state under room temperature.<sup>31</sup> To obtain the predicted crystalline samples with regular ZGNRs, multidimensional pressure–temperature–composition space needs to be explored theoretically in advance. So far, all theoretical high-pressure investigations have been conducted at zero temperature, ignoring the temperature effects.<sup>27–30</sup> Actually, the temperature not only determines the  $TS$  term where  $T$  is the temperature and  $S$  is the entropy in Gibbs energy but also affects volumes ( $V$ ) and energies ( $E$ ), that is,  $E$ ,  $TS$ , and  $PV$  ( $P$  represents the pressure) terms are coupled, which can affect the phase stability and chemical reactions. Here, we employed quasi-harmonic approximation (QHA) theoretical calculations and high-pressure high-temperature (HPHT) experiments to reveal the phase transition tendency of the Li–C system under high temperature and high pressure. Several successful examples show the correction and universality of QHA for the HPHT situation.<sup>32–34</sup> The lithium graphenide  $\text{LiC}_2$  and lithium polyacene  $\text{Li}_3\text{C}_4$  (ZGNRs  $n = \infty$  and 2, respectively) were predicted under HPHT and then confirmed by in situ X-ray diffraction (XRD). Our research indicates that HPHT synthesis is an effective method to construct an ultranarrow GNR structure with defined edges and widths.

## ■ COMPUTATIONAL AND EXPERIMENTAL METHODS

Structure relaxations were performed using density functional theory (DFT) within the Perdew–Burke–Ernzerhof (PBE) functional<sup>35</sup> in the framework of the all-electron projector augmented wave (PAW) method,<sup>36</sup> as implemented in the VASP code.<sup>37</sup> We used a plane-wave kinetic energy cutoff of

700 eV, and the Brillouin zone was sampled with a resolution of  $2\pi \times 0.03 \text{ \AA}^{-1}$ , which showed excellent convergence of the energy differences, stress tensors, and structural parameters.

The variable compound evolutionary algorithm USPEX,<sup>38</sup> used here for predicting new stable structures, searches for the lowest-enthalpy structures at a given pressure. Structure relaxations were performed using DFT within the PBE functional in the framework of the all-electron PAW method, as implemented in the VASP code. The first generation of structures was created randomly. All structures were relaxed at constant pressure and 0 K, and the enthalpy was used as fitness. The energetically worst structures (40%) were discarded and a new generation was created, 30% randomly and 70% from the lowest-enthalpy structures through heredity, lattice mutation, and transmutation. For the QHA calculation, phonon calculations were performed for all promising structures using the PHONOPY code.<sup>39</sup> The super cells of  $3 \times 3 \times 3$ ,  $2 \times 2 \times 2$ ,  $2 \times 2 \times 4$ ,  $2 \times 2 \times 2$ ,  $1 \times 3 \times 4$ ,  $3 \times 3 \times 2$ ,  $2 \times 3 \times 1$ , and  $4 \times 4 \times 3$  are used for C,  $\text{Li}_2\text{C}_2$ ,  $\text{Li}_2\text{C}_3$ ,  $\text{Li}_2\text{C}$ ,  $\text{Li}_3\text{C}_4$ ,  $\text{Li}_4\text{C}_3$ ,  $\text{Li}_5\text{C}_8$ , and  $\text{LiC}_2$ , respectively. Each structure is checked to have no imaginary phonon frequencies from 15 to 40 GPa. For each structure, phonons were computed at 31 different volumes to get the equilibrium volume and predict the Gibbs free energy. The Raman frequencies of the lithium carbides were calculated by vasp\_raman pyvr at 27 GPa.<sup>40</sup>

The  $\text{Li}_2\text{C}_2$  sample was synthesized from the stoichiometric mixture of the Li metal and graphite powder, which was sealed inside a tantalum tube in a glovebox. The tube was then sealed inside an evacuated quartz tube and heated at 800 °C for 12 h. Phase analysis was performed by powder XRD on a Bruker D8 ADVANCE diffractometer (Cu  $K\alpha$  radiation), and no significant impurities were detected (Figure S1). In situ HPHT XRD experiments were carried out at the 16-ID-B beamline at the Advanced Photon Source (APS), Argonne National Laboratory. A diamond anvil cell (DAC) with a diamond culet size of 300  $\mu\text{m}$  in diameter was used to apply pressure. Tungsten gaskets were preindented to a thickness of 30  $\mu\text{m}$ , and the center holes with 180  $\mu\text{m}$  diameters were drilled to act as the sample chamber.  $\text{Li}_2\text{C}_2$  powder was loaded in a glovebox, and Ar was loaded to improve thermal insulation and quasi-hydrostatic pressure conditions. Ruby fluorescence was used for pressure calibration.<sup>41</sup> After Ar was loaded, the sample was checked using Raman spectroscopy and was proved to be  $\text{Li}_2\text{C}_2$ .<sup>31</sup> Then, it was compressed to 27.5 GPa for the HPHT experiments. Another DAC was prepared by using the above-described method and was compressed to 36.5 GPa for the HPHT experiments. To generate high temperatures, the samples were heated on both sides using an infrared laser. The temperature from each side was estimated by collecting the emitted thermal radiation, correcting for the optical system response and fitting the spectral data to Planck's equation. The temperatures used were recorded from the upstream side of the DAC. The X-ray patterns were collected during laser

heating using a CCD detector calibrated with a  $\text{CeO}_2$  standard sample. The wavelength of the incident X-ray was 0.4066 Å. The preliminary data were reduced using the Dioptas program,<sup>42</sup> and the background of the XRD patterns was subtracted. After the in situ XRD experiment, Raman spectra were measured at room temperature without changing the pressure. The wavelength of the incident laser is 488 nm.

## RESULTS AND DISCUSSION

First, we used USPEX<sup>38</sup> to predict the thermodynamically stable Li–C phases and obtain the convex hull at 0 K under 27.5 and 36.5 GPa, respectively (Figure 2a,b), which is

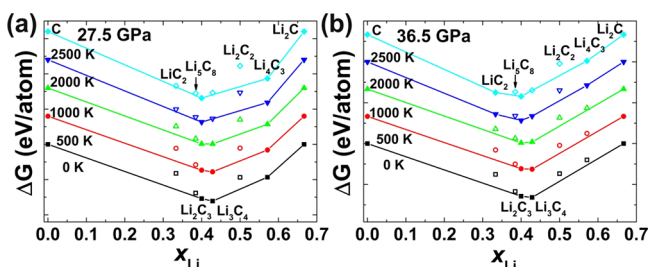


**Figure 2.** Convex hull of the Li–C system at (a) 27.5 and (b) 36.5 GPa at different temperatures, which are shifted by 0.08 eV/atom. The solid symbols represent thermal stable phases, that is, on the convex hull line. The open symbols represent metastable phases. The  $x_{\text{Li}}$  represents the atomic concentration of lithium in the compound  $\text{Li}_m\text{C}_n$ , which is defined as  $x_{\text{Li}} = m/m + n$ .

consistent with the literature.<sup>29</sup>  $\text{Li}_2\text{C}_3$  and  $\text{Li}_3\text{C}_4$  are predicted to be stable at 27.5 and 36.5 GPa, respectively, at 0 K, and  $\text{Li}_4\text{C}_3$  is stable at 27.5 GPa. Their crystal structures and phonon spectra are also presented in Table S1 and Figure S2, respectively, with no imaginary frequency discovered. Then, we used the QHA method to study the Gibbs free energies of all candidate phases including C,  $\text{LiC}_2$ ,  $\text{Li}_2\text{C}_3$ ,  $\text{Li}_3\text{C}_4$ ,  $\text{Li}_2\text{C}_2$ ,  $\text{Li}_4\text{C}_3$ , and  $\text{Li}_6\text{C}_3(\text{Li}_2\text{C})$ , to evaluate their thermodynamic stabilities at HPHT. As shown in Figure 2, both the convex hulls at 27.5 and 36.5 GPa vary significantly from 0 to 2500 K. With increasing temperature,  $\text{LiC}_2$  becomes more stable, whereas  $\text{Li}_3\text{C}_4$  is less stable.

On the basis of Gibbs free energies calculated under HPHT, we summarize the phase diagram of the carbon-rich phases,  $\text{LiC}_2$ ,  $\text{Li}_3\text{C}_4$ , and  $\text{Li}_2\text{C}_3$ , in Figure 3.  $\text{Li}_2\text{C}_3$  is predicted to be stable in the whole investigated area.  $\text{LiC}_2$  becomes thermodynamically stable at HPHT. The transition temperature to  $\text{LiC}_2$  is 2334 K at 29 GPa and decreases to 1410 K at 40 GPa.  $\text{Li}_3\text{C}_4$  (Li polyacene) will decompose at high temperature. The decomposition temperature is 1516 K at 20 GPa and linearly increases to 2665 K at 40 GPa.

Thus, the two decomposition lines of  $\text{LiC}_2$  and  $\text{Li}_3\text{C}_4$  divide the phase diagram into four zones. At low temperature (zone IV),  $\text{Li}_3\text{C}_4$  is stable and  $\text{LiC}_2$  is decomposed, which is consistent with previous theoretical calculations.<sup>29</sup> At low pressure and high temperature (zone II), both  $\text{Li}_3\text{C}_4$  and  $\text{LiC}_2$  decompose. Under high pressure and intermediate temperature,  $\text{Li}_3\text{C}_4$  and  $\text{LiC}_2$  coexist (zone III). The last zone (zone I) is for intermediate pressure and high temperature, where  $\text{Li}_3\text{C}_4$  decomposes and  $\text{LiC}_2$  is stable. The QHA calculations suggest that high temperature promotes polymerization and stabilizes wider GNR or carbon slices.

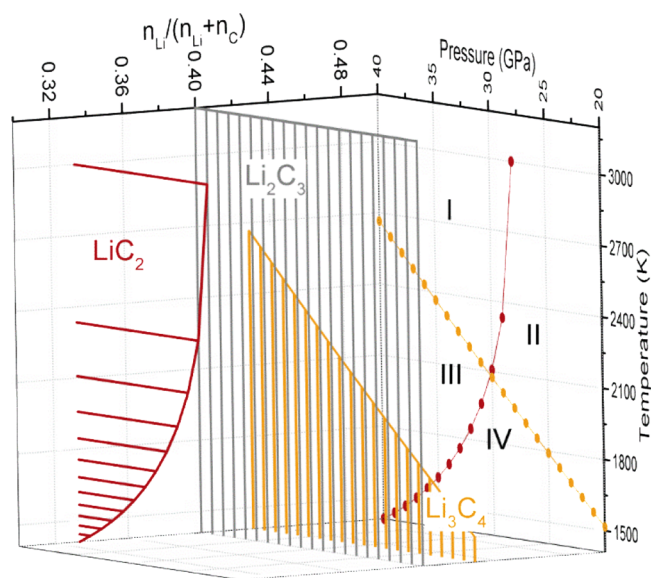


**Figure 3.** Calculated phase diagram of  $\text{LiC}_2$ ,  $\text{Li}_2\text{C}_3$ , and  $\text{Li}_3\text{C}_4$  by QHA. The red, gray, and orange shadings represent the thermodynamic stable  $P$ – $T$  regions of  $\text{LiC}_2$ ,  $\text{Li}_2\text{C}_3$ , and  $\text{Li}_3\text{C}_4$ , respectively. The decomposition lines of  $\text{LiC}_2$  and  $\text{Li}_3\text{C}_4$  are projected on the  $P$ – $T$  plane (red and orange line). The orange line represents the decomposition line of  $6\text{Li}_3\text{C}_4 = 7\text{Li}_2\text{C}_3 + \text{Li}_4\text{C}_3$ , whereas the red line represents the decomposition line of  $2\text{LiC}_2 = \text{Li}_2\text{C}_3 + \text{C}$ . In zones I and III,  $\text{LiC}_2$  is stable, and in zones III and IV,  $\text{Li}_3\text{C}_4$  is stable.

This phenomenon results from the structural features of these Li GNRs. For  $\text{Li}_3\text{C}_4$ , carbon atoms are connected along the ribbon by C–C covalent bonds. In the other two directions perpendicular to the ribbon, the atoms are connected by the ionic interactions between the GNR and Li cations. For comparison,  $\text{LiC}_2$  (Li graphenide) has a 2D covalent-bond sheet and ionic interaction between Li and the graphene sheet in the third direction.<sup>43</sup> Compared to ionic bonds, covalent bonds are harder to stretch with temperature, so  $\text{LiC}_2$  has a smaller thermal expansion coefficient and a smaller volume increase at high temperature and becomes energetically favored under high pressure.

To confirm these predicted structures, we conducted in situ HPHT XRD experiments. Crystalline powder  $\text{Li}_2\text{C}_2$  was compressed to 27.5 and 36.5 GPa, respectively, at room temperature and heated up (Figure 4a,b). As shown in Figure 4a, at 27.5 GPa and room temperature, most of  $\text{Li}_2\text{C}_2$  transforms to the amorphous state, and only some residues are left (the blue arrows in Figure 4a). Most of the XRD peaks were ascribed to Ar and  $\text{Li}_2\text{O}$  (black and red arrows in Figure 4a). When heated up, several new peaks arose (represented by the asterisks) and indicated the formation of crystalline phase(s). By comparing the diffraction patterns collected under high temperature, we selected a pattern (1696 K) with sharp diffraction peaks and minor impurities. These diffraction peaks were indexed with a hexagonal  $P6/mmm$  lattice,  $a = b = 2.49193(13)$  Å and  $c = 3.3823(2)$  Å. By performing a series of crystallographic analysis, the crystallized phase was determined as Li graphenide ( $\text{LiC}_2$ , Figure 1), and the Rietveld refinement plot is shown in Figure 5a.

At 36.5 GPa,  $\text{Li}_2\text{C}_2$  also experienced a similar process. New peaks (indicated by the asterisks in Figure 4b) gradually emerged above 1400 K and became stable when heated up to above 1800 K, which indicates a thermodynamic equilibrium.

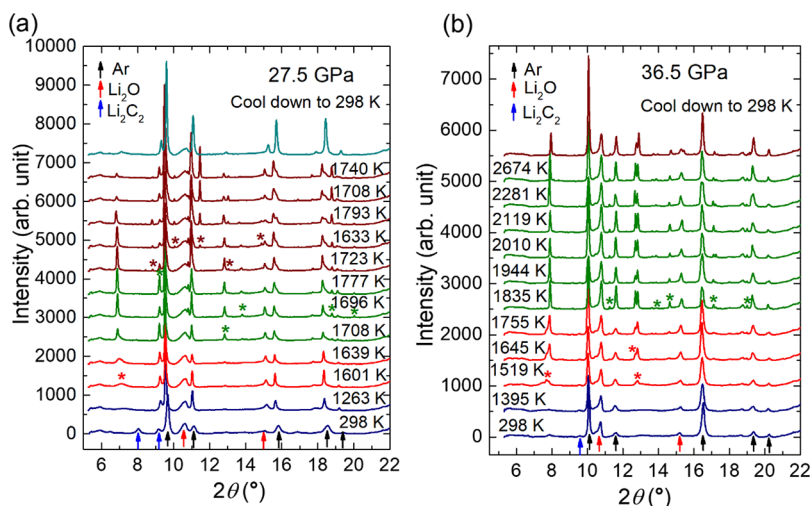


**Figure 4.** Selected in situ XRD patterns of  $\text{Li}_2\text{C}_2$  under (a) 27.5 and (b) 36.5 GPa at high temperature. The wavelength of the incident X-ray is 0.4066 Å. The patterns are sequentially stacked up with increasing time and power. The asterisks (\*) represent the new peaks. Ar is the pressure-transmitting medium, and  $\text{Li}_2\text{O}$  is the impurity introduced while loading  $\text{Li}_2\text{C}_2$  into DAC.

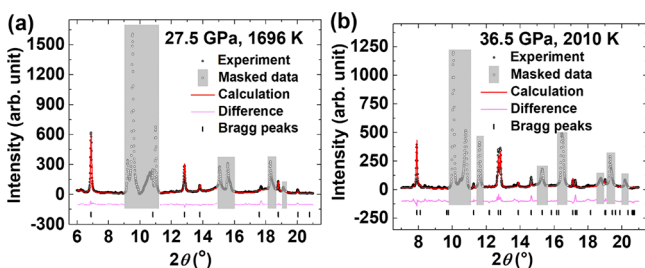


**Figure 5.** Rietveld refinement plots of (a)  $\text{Li}_2\text{C}_2$  and (b)  $\text{Li}_3\text{C}_4$  under 27.5 GPa, 1696 K and 36.5 GPa, 2010 K, respectively. The wavelength of the incident X-ray is 0.4066 Å. The peaks coming from Ar and  $\text{Li}_2\text{O}$  were masked.

After cooling down, the peaks are maintained, indicating that the new phase is stable at room temperature. By comparing the diffraction patterns to those of the predicted phases, we found that the predicted  $\text{Li}_3\text{C}_4$  (*Immm*) phase fits the XRD pattern (36.5 GPa and 2010 K) very well.<sup>29</sup> The Rietveld refinement results are shown in Figure 5b, and the lattice parameters are  $a = 11.4944$  Å,  $b = 3.0525$  Å, and  $c = 2.464$  Å. As shown in Figure 6a, the carbon atoms in  $\text{Li}_3\text{C}_4$  polymerize into polyacene, the nanoribbon with two zigzag chains, which is referred to as the first-order structural unit. The Li cations are closely fitted between the (half) six-membered rings of neighboring ribbons, connecting the ribbons together and forming a second-order structural unit (the purple region in Figure 6a), which is neutral in charge. These Li cations form rectangular lattices as shown in the dashed line in Figure 6a. When the second-order structural units are stacked, the Li cations between the (half) six-membered rings are against the centers of the neighboring Li rectangles, that is, the negatively

charged secondary carbon is located on the edge of GNR. Actually, this Li–C (1.957 Å) distance is even shorter than the nearest Li–Li distance (2.301 Å) between the neighboring second-order units (Figure 6a), which is likely to result from significant electrostatic attraction and hence stabilizes the whole crystal.

Nominally, the C atom in  $\text{Li}_3\text{C}_4$  has an oxidation state of 3/4 supposing Li keeps +1. Theoretical calculation shows that the carbon atoms on the edge and in the middle have Bader charges of  $-0.76$  and  $-0.45$ , respectively, whereas the Li atoms have Bader charges of  $+0.81$ .  $\text{Li}_3\text{C}_4$  is predicted to be metallic with a conductive charged GNR, as shown in Figure 6b. The nonintegral oxidation state of carbon suggests an important rule under high pressure: effective stacking becomes more important compared to a traditional stoichiometry/integral oxidation state.

A metastable  $\text{Li}_2\text{C}_2$  polyacene GNR phase was also predicted, as shown in Figure 7.<sup>29</sup> It has a similar second-order structural unit with  $\text{Li}_3\text{C}_4$ , but with another layer of Li between them (indicated by the dashed circles in Figure 7), which may be responsible for the instability. Its fragment was identified when compressed under room temperature.<sup>31</sup> By comparing the structural similarities of this  $\text{Li}_2\text{C}_2$  and  $\text{Li}_3\text{C}_4$ , we propose the following reaction process:  $\text{C}_2^{2-}$  in  $\text{Li}_2\text{C}_2$  tends to polymerize under external pressure and forms ZGNR fragments in amorphous  $\text{Li}_2\text{C}_2$  at room temperature. When heated up, the fragments start to connect to form ZGNRs, 1/4 of Li is excluded, and the Li GNRs are crystallized in the most energetically preferred structure,  $\text{Li}_3\text{C}_4$ .

It is worth noting that the predicted  $\text{Li}_2\text{C}_3$  was not observed in our experiment. From thermodynamic rules, when  $\text{Li}_3\text{C}_4$  is thermodynamically stable,  $\text{Li}_2\text{C}_3$  should not appear in the

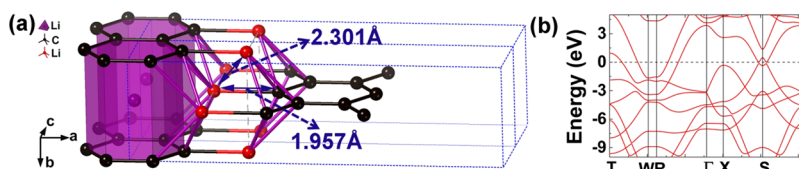


**Figure 6.** (a) Crystal and (b) band structure of  $\text{Li}_3\text{C}_4$ .

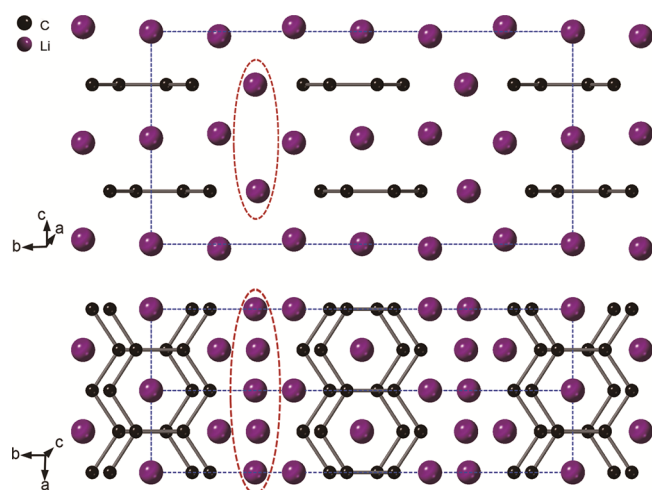


Figure 7. Crystal structure of  $\text{Li}_2\text{C}_2$ - $Cmcm$ -ribbon phase.<sup>29</sup>

sample with  $\text{Li}/\text{C} = 1:1$ . However, at 27.5 GPa, we observed  $\text{LiC}_2$ , whose composition deviates even further away from 1:1. This is most likely due to compositional segregation. A significant amount of Li atoms may migrate outside the laser irradiation (and hence incident X-ray beam), and the composition left is carbon-rich. The possible reason of migration may include temperature and pressure gradient, which is still under investigation.

We also characterized the samples using Raman spectroscopy. The sample under 27.5 GPa does not show obvious features but high background (Figure 8). The sample under

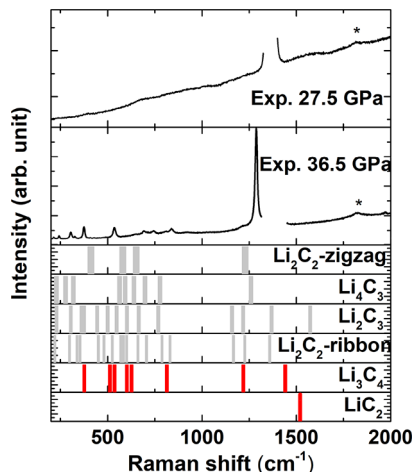


Figure 8. Raman spectra of the heated  $\text{Li}_2\text{C}_2$  samples ( $\text{LiC}_2$  and  $\text{Li}_3\text{C}_4$ ) under high pressure. The Raman peak of the diamond is masked, and the peaks marked by asterisks are from the anvils.

36.5 GPa shows a series of peaks below  $1300\text{ cm}^{-1}$ , with the strongest peak at  $\sim 1288\text{ cm}^{-1}$ . We calculated the Raman spectra of several lithium carbides and selected those with peaks in the range of  $1200\text{--}1350\text{ cm}^{-1}$  for comparison. Most of these carbides are polycarbides with ribbon ( $\text{Li}_2\text{C}_2$  ribbon,  $\text{Li}_3\text{C}_4$ ,  $\text{Li}_2\text{C}_3$ , and  $\text{LiC}_2$ ) or chain structures ( $\text{Li}_2\text{C}_2$  zigzag,  $\text{Li}_4\text{C}_3$ ), and this peak most likely indicates the ribbon structure. Among them,  $\text{Li}_3\text{C}_4$  is the best candidate, though other phases cannot be excluded. This supports our discovery using in situ XRD. For  $\text{LiC}_2$ , only one peak at  $1520\text{ cm}^{-1}$  is predicted, and it

is not surprising that it was not observed because  $\text{LiC}_2$  is metallic.

In the current experiment, we tested two  $P$ - $T$  points and observed the two members of  $\text{Li}_{n+1}\text{C}_{2n}$  with  $n = 2$  and  $\infty$ . We can expect more Li ZGNRs with various widths, by testing more points between 27.5 and 36.5 GPa and between 300 and 2200 K and by controlling the ratio of Li and carbon, temperature gradient, time, rate of heating, and so on. On one hand, the ZGNRs in  $\text{Li}_{n+1}\text{C}_{2n}$  have identical edges. When lithium is removed, pure ultranarrow ZGNRs would be obtained. On the other hand, these Li GNRs have negative charges on the ribbons, which suggests that they are very good nucleophilic reagents and very easy to react with protic solvents including water and alcohol or other reagents with a positive charge. This will be a useful method to obtain a neutral ZGNR with controlled atomic width and will also be a method to synthesize functionalized GNRs.

In conclusion, we have theoretically predicted and experimentally synthesized two phases containing ZGNR structures, graphene compounds  $\text{LiC}_2$  and polyacene  $\text{Li}_3\text{C}_4$  by subjecting  $\text{Li}_2\text{C}_2$  under HPHT conditions using the technique of laser-heated DAC. Their crystal structures under HPHT have been determined as closely packed ZGNR and  $\text{Li}^+$ , in agreement with ab initio Gibbs free-energy calculation by QHA. On the basis of the calculation, several Li ZGNRs with a stoichiometric ratio of  $\text{Li}_{n+1}\text{C}_{2n}$  have also been investigated, which are the intermediate phases between lithium polyacene  $\text{Li}_3\text{C}_4$  and lithium graphenide  $\text{LiC}_2$ . It is expected that with precise control of temperature and pressure, we can obtain lithium ZGNRs with an expected width, which will shed light on the “bottom-up” synthesis of ZGNRs with atomic ordering and a controlled width.

## ■ ASSOCIATED CONTENT

### 📄 Supporting Information

The Supporting Information is available free of charge on the ACS Publications website at DOI: 10.1021/acs.jpcc.8b04081.

XRD pattern of synthesized  $\text{Li}_2\text{C}_2$  raw material; phonon spectrum of  $\text{Li}_2\text{C}_3$  and  $\text{Li}_3\text{C}_4$  at 30 GPa; and crystal structures of the optimized  $\text{Li}_2\text{C}_2$ ,  $\text{Li}_3\text{C}_4$ , and  $\text{Li}_2\text{C}_3$  phases (PDF)

## ■ AUTHOR INFORMATION

### Corresponding Authors

\*E-mail: likuo@hpstar.ac.cn (K.L.).

\*E-mail: zhenghy@hpstar.ac.cn (H.Z.).

### ORCID

Kuo Li: 0000-0002-4859-6099

Haiyan Zheng: 0000-0002-4727-5912

### Author Contributions

X.D. and L.W. contributed equally. The manuscript was written through contributions of all authors. All authors have given approval to the final version of the manuscript.

### Notes

The authors declare no competing financial interest.

## ■ ACKNOWLEDGMENTS

The authors acknowledge the support of the National Natural Science Foundation of China (NSFC) (grant nos. 21771011, 21501162, and 21601007). The authors also acknowledge the support from the Top 1000-Talents Award. A portion of this

research was performed at HPCAT (Sector 16), Advanced Photon Source (APS), Argonne National Laboratory. HPCAT operations are supported by DOE-NNSA under award no. DE-NA0001974, with partial instrumentation funding by NSF. Y.M. acknowledges the support of DOE-BES/DMSE under award no. DE-FG02-99ER45775. APS is supported by DOE-BES, under contract no. DE-AC02-06CH11357. The calculation was performed on the TianheII supercomputer at Chinese National Supercomputer Center in Guangzhou.

## REFERENCES

- (1) Li, X.; Wang, X.; Zhang, L.; Lee, S.; Dai, H. Chemically Derived, Ultrasmooth Graphene Nanoribbon Semiconductors. *Science* **2008**, *319*, 1229–1232.
- (2) Silveiro, I.; Ortega, J. M. P.; de Abajo, F. J. G. Quantum nonlocal effects in individual and interacting graphene nanoribbons. *Light. Sci. Appl.* **2015**, *4*, No. e241.
- (3) Son, Y.-W.; Cohen, M. L.; Louie, S. G. Half-metallic Graphene Nanoribbons. *Nature* **2006**, *444*, 347–349.
- (4) Yang, L.; Park, C.-H.; Son, Y.-W.; Cohen, M. L.; Louie, S. G. Quasiparticle Energies and Band Gaps in Graphene Nanoribbons. *Phys. Rev. Lett.* **2007**, *99*, 186801.
- (5) Ritter, K. A.; Lyding, J. W. The Influence of Edge Structure on the Electronic Properties of Graphene Quantum Dots and Nanoribbons. *Nat. Mater.* **2009**, *8*, 235–242.
- (6) Barone, V.; Hod, O.; Scuseria, G. E. Electronic Structure and Stability of Semiconducting Graphene Nanoribbons. *Nano Lett.* **2006**, *6*, 2748–2754.
- (7) Kimouche, A.; Ervasti, M. M.; Drost, R.; Halonen, S.; Harju, A.; Joensuu, P. M.; Sainio, J.; Liljeroth, P. Ultra-narrow Metallic Armchair Graphene Nanoribbons. *Nat. Commun.* **2015**, *6*, 10177.
- (8) Llinas, J. P.; Fairbrother, A.; Barin, G. B.; Shi, W.; Lee, K.; Wu, S.; Choi, B. Y.; Braganza, R.; Lear, J.; Kau, N.; et al. Short-channel Field-effect Transistors with 9-atom and 13-atom Wide Graphene Nanoribbons. *Nat. Commun.* **2017**, *8*, 633.
- (9) Talirz, L.; Söde, H.; Dumschlaff, T.; Wang, S.; Sanchez-Valencia, J. R.; Liu, J.; Shinde, P.; Pignedoli, C. A.; Liang, L.; Meunier, V.; et al. On-surface Synthesis and Characterization of 9-Atom Wide Armchair Graphene Nanoribbons. *ACS Nano* **2017**, *11*, 1380–1388.
- (10) Plumb, L.; Zhang, L.; Wang, X.; Diankov, G.; Dai, H. Narrow Graphene Nanoribbons from Carbon Nanotubes. *Nature* **2009**, *458*, 877–880.
- (11) Kosynkin, D. V.; Higginbotham, A. L.; Sinitskii, A.; Lomeda, J. R.; Dimiev, A.; Price, B. K.; Tour, J. M. Longitudinal Unzipping of Carbon Nanotubes to form Graphene Nanoribbons. *Nature* **2009**, *458*, 872–876.
- (12) Kosynkin, D. V.; Lu, W.; Sinitskii, A.; Pera, G.; Sun, Z.; Tour, J. M. Highly Conductive Graphene Nanoribbons by Longitudinal Splitting of Carbon Nanotubes Using Potassium Vapor. *ACS Nano* **2011**, *5*, 968–974.
- (13) Chen, L.; Hernandez, Y.; Feng, X.; Müllen, K. From Nanographene and Graphene Nanoribbons to Graphene Sheets: Chemical Synthesis. *Angew. Chem., Int. Ed.* **2012**, *51*, 7640–7654.
- (14) Qian, H.; Negri, F.; Wang, C.; Wang, Z. Fully Conjugated Tri(perylene bisimides): An Approach to the Construction of n-Type Graphene Nanoribbons. *J. Am. Chem. Soc.* **2008**, *130*, 17970–17976.
- (15) Yang, W.; Lucotti, A.; Tommasini, M.; Chalifoux, W. A. Bottom-up Synthesis of Soluble and Narrow Graphene Nanoribbons Using Alkyne Benzannulations. *J. Am. Chem. Soc.* **2016**, *138*, 9137–9144.
- (16) Cai, J.; Ruffieux, P.; Jaafar, R.; Bieri, M.; Braun, T.; Blankenburg, S.; Muoth, M.; Seitsonen, A. P.; Saleh, M.; Feng, X.; et al. Atomically Precise Bottom-up Fabrication of Graphene Nanoribbons. *Nature* **2010**, *466*, 470–473.
- (17) Müllen, A.; Feng, X.; Hernandez, Y.; Jensen, S. A.; Bonn, M.; Yang, H.; Verzhbitskiy, I. A.; Casiraghi, C.; Hansen, M. R.; Koch, A. H. R.; et al. Synthesis of Structurally Well-defined and Liquid-phase-processable Graphene Nanoribbons. *Nat. Chem.* **2014**, *6*, 126–132.
- (18) Fytas, E. K.; Sakellariou, G.; Vougioukalakis, G. C. Chemical Synthesis of Graphene Nanoribbons. *Arkivoc* **2015**, *2015*, 167–192.
- (19) Liu, J.; Li, B.-W.; Tan, Y.-Z.; Giannakopoulos, A.; Sanchez-Sanchez, C.; Beljonne, D.; Ruffieux, P.; Fasel, R.; Feng, X.; Müllen, K. Toward Cove-edged Low Band Gap Graphene Nanoribbons. *J. Am. Chem. Soc.* **2015**, *137*, 6097–6103.
- (20) Ruffieux, P.; Wang, S.; Yang, B.; Sánchez-Sánchez, C.; Liu, J.; Dienel, T.; Talirz, L.; Shinde, P.; Pignedoli, C. A.; Passerone, D.; et al. On-surface Synthesis of Graphene Nanoribbons with Zigzag Edge Topology. *Nature* **2016**, *531*, 489–492.
- (21) Einholz, R.; Fang, T.; Berger, R.; Grüninger, P.; Früh, A.; Chassé, T.; Fink, R. F.; Bettinger, H. F. Heptacene: Characterization in Solution, in the Solid State, and in Films. *J. Am. Chem. Soc.* **2017**, *139*, 4435–4442.
- (22) Watanabe, M.; Chang, Y. J.; Liu, S.-W.; Chao, T.-H.; Goto, K.; Islam, M. M.; Yuan, C.-H.; Tao, Y.-T.; Shinmyozu, T.; Chow, T. J. The Synthesis, Crystal Structure and Charge-Transport Properties of Hexacene. *Nat. Chem.* **2012**, *4*, 574–578.
- (23) Zade, S. S.; Bendikov, M. Heptacene and Beyond: the Longest Characterized Acenes. *Angew. Chem., Int. Ed.* **2010**, *49*, 4012–4015.
- (24) Shen, B.; Tatchen, J.; Sanchez-Garcia, E.; Bettinger, H. F. Evolution of the Optical Gap in the Acene Series: Undecacene. *Angew. Chem., Int. Ed.* **2018**, *57*, 10506–10509.
- (25) Presser, V.; Heon, M.; Gogotsi, Y. Carbide-Derived Carbons - From Porous Networks to Nanotubes and Graphene. *Adv. Funct. Mater.* **2011**, *21*, 810–833.
- (26) Kim, D. Y.; Stefanoski, S.; Kurakevych, O. O.; Strobel, T. A. Synthesis of an Open-framework Allotrope of Silicon. *Nat. Mater.* **2015**, *14*, 169–173.
- (27) Li, Y.-L.; Luo, W.; Zeng, Z.; Lin, H.-Q.; Mao, H.-k.; Ahuja, R. Pressure-induced superconductivity in CaC<sub>2</sub>. *Proc. Natl. Acad. Sci. U.S.A.* **2013**, *110*, 9289–9294.
- (28) Li, Y.-L.; Wang, S.-N.; Oganov, A. R.; Gou, H.; Smith, J. S.; Strobel, T. A. Investigation of Exotic Stable Calcium Carbides using Theory and Experiment. *Nat. Commun.* **2015**, *6*, 6974.
- (29) Lin, Y.; Strobel, T. A.; Cohen, R. E. Structural Diversity in Lithium Carbides. *Phys. Rev. B: Condens. Matter Mater. Phys.* **2015**, *92*, 214106.
- (30) Benson, D.; Li, Y.; Luo, W.; Ahuja, R.; Svensson, G.; Häussermann, U. Lithium and Calcium Carbides with Polymeric Carbon Structures. *Inorg. Chem.* **2013**, *52*, 6402–6406.
- (31) Wang, L.; Dong, X.; Wang, Y.; Zheng, H.; Li, K.; Peng, X.; Mao, H.-k.; Jin, C.; Meng, Y.; Huang, M.; et al. Pressure-Induced Polymerization and Disproportionation of Li<sub>2</sub>C<sub>2</sub> Accompanied with Irreversible Conductivity Enhancement. *J. Phys. Chem. Lett.* **2017**, *8*, 4241–4245.
- (32) López-Moreno, S.; Errandonea, D.; Rodríguez-Hernández, P.; Muñoz, A. Polymorphs of CaSeO<sub>4</sub> under Pressure: A First-Principles Study of Structural, Electronic, and Vibrational Properties. *Inorg. Chem.* **2015**, *54*, 1765–1777.
- (33) López-Moreno, S.; Rodríguez-Hernández, P.; Muñoz, A.; Errandonea, D. First-Principles Study of InVO<sub>4</sub> under Pressure: Phase Transitions from CrVO<sub>4</sub> to AgMnO<sub>4</sub>-Type Structure. *Inorg. Chem.* **2017**, *56*, 2697–2711.
- (34) López-Moreno, S.; Errandonea, D. Ab Initio Prediction of Pressure-induced Structural Phase Transitions of CrVO<sub>4</sub>-type Orthophosphates. *Phys. Rev. B: Condens. Matter Mater. Phys.* **2012**, *86*, 104112.
- (35) Perdew, J. P.; Burke, K.; Ernzerhof, M. Generalized Gradient Approximation Made Simple. *Phys. Rev. Lett.* **1996**, *77*, 3865–3868.
- (36) Blöchl, P. E. Projector Augmented-wave Method. *Phys. Rev. B: Condens. Matter Mater. Phys.* **1994**, *50*, 17953–17979.
- (37) Kresse, G.; Furthmüller, J. Efficiency of Ab-initio Total Energy Calculations for Metals and Semiconductors Using a Plane-wave Basis Set. *Comput. Mat. Sci.* **1996**, *6*, 15–50.
- (38) Oganov, A. R.; Glass, C. W. Crystal Structure Prediction Using Ab Initio Evolutionary Techniques: Principles and Applications. *J. Chem. Phys.* **2006**, *124*, 244704.

- (39) Togo, A.; Oba, F.; Tanaka, I. First-principles Calculations of the Ferroelastic Transition between Rutile-type and  $\text{CaCl}_2$ -type  $\text{SiO}_2$  at High Pressures. *Phys. Rev. B: Condens. Matter Mater. Phys.* **2008**, *78*, 134106.
- (40) Fonari, A.; Stauffer, S. in *vasp\_raman.py*. <https://github.com/raman-sc/VASP/>, 2013.
- (41) Mao, H. K.; Xu, J.; Bell, P. M. Calibration of the Ruby Pressure Gauge to 800 kbar under Quasi-hydrostatic Conditions. *J. Geophys. Res.: Solid Earth* **1986**, *91*, 4673–4676.
- (42) Prescher, C.; Prakapenka, V. B. DIOPTAS: a Program for Reduction of Two-dimensional X-ray Diffraction Data and Data Exploration. *High Pressure Res* **2015**, *35*, 223–230.
- (43) Mordkovich, V. Z. Synthesis and XPS Investigation of Superdense Lithium-graphite Intercalation Compound,  $\text{LiC}_2$ . *Synth. Met.* **1996**, *80*, 243–247.